HHS Public Access

Author manuscript

Dev Biol. Author manuscript; available in PMC 2018 October 15.

Published in final edited form as:

Dev Biol. 2011 December 01; 360(1): 110–122. doi:10.1016/j.ydbio.2011.09.011.

Nephron formation adopts a novel spatial topology at cessation of nephrogenesis

Bree A. Rumballe[1], **Kylie M. Georgas**[1], **Alexander N. Combes**[1], **Adler L. Ju**[1], **Thierry Gilbert**[2], and **Melissa H. Little**[1,#]

[1]Institute for Molecular Bioscience, The University of Queensland, St. Lucia, Brisbane, Australia, 4072

[2]Centre for Developmental Biology, UMR5547, University Paul Sabatier, Toulouse, France

Abstract

Nephron number in the mammalian kidney is known to vary dramatically, with postnatal renal function directly influenced by nephron complement. What determines final nephron number is poorly understood but nephron formation in the mouse kidney ceases within the first few days after birth, presumably due to the loss of all remaining nephron progenitors via epithelial differentiation. What initiates this event is not known. Indeed, whether nephron formation occurs in the same way at this time as during embryonic development has also not been examined. In this study, we investigate the key cellular compartments involved in nephron formation; the ureteric tip, cap mesenchyme and early nephrons; from postnatal day (P) 0 to 6 in the mouse. High resolution analyses of gene and protein expression indicate that loss of nephron progenitors precedes loss of ureteric tip identity, but show spatial shifts in the expression of cap mesenchyme genes during this time. In addition, cap mesenchymal volume and rate of proliferation decline prior to birth. Section-based 3D modeling and Optical Projection Tomography revealed a burst of ectopic nephron induction, with the formation of multiple (up to 5) nephrons per ureteric tip evident from P2. While the distal-proximal patterning of these nephrons occurred normally, their spatial relationship with the ureteric compartment was altered. We propose that this phase of nephron formation represents an acceleration of differentiation within the cap mesenchyme due to a displacement of signals within the nephrogenic niche.

Keywords

nephron induction; nephrogenesis; kidney development; morphogenesis; cap mesenchyme; ureteric tip; gene expression; 3D modeling; confocal microscopy; optical projection tomography

[#]**Corresponding Author:** Professor Melissa H Little, NHMRC Principal Research Fellow, Institute for Molecular Bioscience, The University of Queensland, St. Lucia, 4072, Australia.

Introduction

The nephrons of the kidney arise from an embryonic nephron progenitor population within the periphery of the mammalian kidney referred to as the cap mesenchyme (Boyle et al, 2008; Kobayashi et al, 2008). Self-renewal of this population requires a specific spatial relationship with the adjacent ureteric tip epithelium and is likely also influenced by other surrounding cellular compartments. The cap mesenchyme (CM) is marked by the expression of key transcriptional regulators (including *Wt1, Cited1, Meox1, Eya1, Pax2, Six2*), some of which are known to be required for commitment, self-renewal, survival and a capacity to form nephrons (reviewed in Hendry et al, 2011). Subtle distinctions in the domains of expression of such genes within the cap mesenchyme suggest that this compartment is a continuum of differentiation with the most uncommitted cells furthest from the newly forming nephrons (Mugford et al, 2009). The CM is closely associated with the tips of the branching ureteric epithelium with reciprocal signaling occurring between these compartments. It is the expression of *Gdnf* by the CM that regulates the proliferation and migration of the ureteric tip cells to ensure continued branching (reviewed in Costantini and Kopan, 2010). Conversely, it is the secretion of the Wnt ligand, Wnt9b, from the ureteric epithelium that initiates the process of nephron formation via mesenchyme to epithelial transition (MET) of the CM (Carroll et al, 2005). This in turn initiates expression of *Fgf8* and *Wnt4* within a pretubular aggregate (Stark et al, 1994; Greishamer et al, 2005; Perantoni et al, 2005). The subsequent MET involves non-canonical autocrine Wnt4 signaling to form an epithelial renal vesicle (Park et al, 2007; Burn et al, 2011; Tanigawa et al, 2011). Immediately prior to epithelialisation, polarized gene expression is evident within the renal vesicle (Georgas et al, 2009), marking the commencement of a complex process of tubule formation, elongation, patterning and segmentation to form the mature nephron (reviewed in Kopan et al, 2007). These newly formed immature epithelial nephrons (with central lumen and partial basement membrane) fuse to the adjacent ureteric tip (late renal vesicle stage) to form a contiguous lumen with the ureteric epithelium, ensuring drainage from the nephron through the collecting ducts to the ureter (Georgas et al, 2009).

The number of nephrons present per organ varies dramatically from 11,000 to 19,000 in mice (Merlet-Benichou et al, 1999) and 200,000 to 1.8 million in humans (Hughson et al, 2003). A final wave of nephrogenesis occurs around birth in mouse (Hartman et al, 2007) and approximately 36 weeks of gestation in humans (Hinchliffe et al, 1991). Critically, it is variation in this final nephron number that can influence renal function with a low nephron number associating with renal disease (Brenner et al, 1992; Luyckx et al, 2010.). It has been assumed that each nephron formation event is the same as the next, irrespective of whether an individual nephron arose early or late in kidney development. The molecular events that govern the end of nephron formation have not been elucidated, although a recent profiling of the nephron progenitor compartment has been performed (Brunskill et al, 2011). While this confirms the timing of cessation of nephrogenesis, it is not clear whether this results from an active trigger around birth or from a gradual decline in nephron progenitors over a longer period of time. Changes in the spatial relationships of these three compartments during this final wave of nephrogenesis have also not been thoroughly investigated due to the imaging challenges of such a large organ.

In this study, we have sought to better characterize the cessation of nephrogenesis at the molecular, cellular and topological level. Section *in situ* hybridization (SISH) for key compartment marker genes was performed from E15.5 to postnatal day (P) 6. While the same genes involved in embryonic nephrogenesis are expressed during cessation, the spatial relationship between the cap mesenchyme, ureteric tips and nephron anlagen during the last wave of nephron induction is unique. CM genes previously regarded as critical for ensuring progenitor self-renewal appear within early nephron subcompartments. In addition, 3D modeling of the nephrogenic niche revealed that multiple, nephrons form per tip during the final wave of induction. Unlike embryonic nephrons, which always originate underneath the ureteric tip and adjacent to the ureteric trunk, these final nephrons surround a single tip resulting in multiple direct connections with the same ureteric tip. The expression of nephron markers and genes previously shown to support progenitor self-renewal within these final nephrons supports a model of rapid differentiation of the nephron progenitor population, highlighting differences between postnatal and embryonic nephrogenesis.

Methods and materials

Tissue collection and processing

The care of all mice and the sacrifice of pregnant females and neonates were carried out according to the ‘Australian Code of Practice for the Care and Use of Animals for Scientific Purposes’ and approved in advance by the University of Queensland Animal Ethics Committee (Molecular Biosciences). Outbred CD1 wildtype mice were time-mated and the kidneys collected from embryos (15.5dpc) or neonatal pups (P0, P2, P4, P6). Mice were left to litter naturally and the day of birth recorded as P0. The average gestational age at parturition for this strain was E19. For procedures requiring standard kidney sections, tissues were fixed in 4% paraformaldehyde in phosphate buffered saline (PBS) overnight at 4 °C, dehydrated using an ethanol series and stored in 70% ethanol at 4 °C. Paraffin embedding and sectioning (7μm) was performed as described previously (Rumballe et al., 2008).

Histology of thin sections (PAS and toluidine blue staining)

For Periodic Acid Schiff’s (PAS) staining, dissected neonatal kidney slices were fixed with alcoholic Bouin’s solution (70% ethanol, 10% formaldehyde, 0.5% picric acid, 7% acetic acid), embedded in paraffin and sectioned at 4 μm. Following standard dewaxing and rehydration, sections were submitted to PAS staining. For toluidine blue staining, kidneys were fixed with 2% glutaraldehyde in 0.1M cacodylate buffer (pH 7.4), epon-embedded, sectioned at 1 μm and stained with toluidine blue. Histology sections were mounted and photographed with Olympus BX51 microscope equipped with digital imaging. Measurements of both nephrogenic and cortical thickness were performed on mid-sagittal sections of neonatal kidneys using 4–5 pups per age group.

Section in situ hybridization

Sectioned kidneys (7μm paraffin) were hybridized with digoxigenin-labelled antisense riboprobes generated using gene-specific PCR (Supplementary Table 1). The complete protocol for riboprobe generation and section in situ hybridization (SISH) has been described in detail previously (Rumballe et al, 2008; Georgas et al 2009) and is available on

the GUDMAP website via Research Protocols (http://www.gudmap.org/Research/Protocols/Little.html). SISH was performed using a Tecan Freedom Evo 150 robot for prehybridization, hybridization of ribobprobes and incubation of tissue with anti-digoxigenin antibody conjugated to alkaline phosphatase. BM Purple color substrate was used for the detection of phosphatase activity. Tissues were post-fixed in 4% paraformaldehyde in PBS for 20 min and mounted with aqueous mounting medium. Sectioned kidneys were photographed using the semi-automated .slide System and OlyVIA software (Soft Imaging Systems, Olympus).

Dual section in situ hybridization/immunohistochemistry

Immunohistochemistry was performed on sectioned kidneys (7μm paraffin) after SISH using anti-Collagen IV antibody (Chemicon International, AB756P) to visualize basement membrane. The protocol has been described previously (Georgas et al, 2008) and utilizes a biotin-conjugated secondary antibody detected with avidin-conjugated horseradish peroxidase and visualized using DAB color substrate. After the color reaction, tissues were fixed in 4% paraformaldehyde in PBS for 20 min and mounted with aqueous mounting medium. Kidney sections were photographed using the semi-automated .slide System and OlyVIA software (Soft Imaging Systems, Olympus).

Section immunofluorescence

Sectioned kidneys (7μm paraffin) were prepared for immunofluorescence by dewaxing and rehydration with an ethanol series using standard protocols, pre-treated using an antigen unmasking procedure and immunofluorescence performed as described previously (Georgas et al, 2009). Primary antibodies; anti-Six2 (Sapphire Bioscience, H00010736-MO1), anti-Collagen IV (Chemicon International, AB756P), anti-CalbindinD28K (Sigma, sc-7672), anti-pHH3 (Millipore, 06–570) and anti-Cyclin D1 (Santa Cruz Biotechnology Inc., sc-450) were diluted (1:100 to 1:250) in 1% heat inactivated sheep serum in PBS and sections incubated overnight at 4 °C. Tissues were incubated with fluorescently-labeled secondary antibodies for 60min at room temperature followed by 5min with DAPI to label nuclei. Sections were mounted with aqueous mounting medium for fluorescence (Vectorshield) and photographed using either a standard fluorescent microscope (Olympus BX51, DP70 color digital camera) or confocal microscope (Zeiss 510 LSM).

Quantitative analysis of cellular proliferation

Cell numbers and levels of proliferation were determined using spot counting algorithms in BitPlane Imaris using images of sectioned kidneys after immunofluorescence with anti-Six2, anti-CalbindinD28K and anti-pHH3 antibodies and DAPI nuclear labeling. Threshold-based spot detection was standardized for each time point. Data is displayed as the mean ± standard error; significance was determined using an unpaired t-test.

3D modeling

Modeling of P2 kidneys was performed as described previously (Georgas et al, 2009; Combes et al, 2009). Serial sections (5μm paraffin) of P2 kidneys were labeled with anti-Calbindin D28K (ureteric tree) and anti-Collagen IV (basement membrane) using

immunofluorescence. Serial sections were photographed using a standard fluorescent microscope and images manually aligned using Adobe Photoshop CS2. Nephron and ureteric tree structures were rendered into 3D models using the tomography program IMOD (http://bio3d.colorado.edu/imod/) (Kremer et al, 1996). Representative 2D images and 3D movies were generated using IMOD and Adobe ImageReady CS2.

Optical Projection Tomography (OPT)

Neonatal kidneys (P0, P2) were dissected as described above and fixed with 4% paraformaldehyde in PBS for 10 minutes and rinsed twice with PBS. The kidneys were then transferred into a tris-buffered saline wash with 0.1% triton-X 100 (TBS-Tx), blocked in TBS-Tx with 1% heat inactivate sheep serum for 1 hour before being incubated overnight at 4°C with anti-CalbindinD28K primary antibody (Sigma Aldrich, C9848, St Louis, MO, USA). After thoroughly washing with TBS-Tx, the kidneys were incubated overnight at 4°C with Alexa Fluor 647 secondary antibody (Invitrogen, A21235, Carlsbad, CA, USA). They were then embedded in 1.5% low melting point agarose and affixed onto metal mounts. The agarose block was trimmed and dehydrated in 100% methanol overnight. The blocks were cleared overnight in a solution of 1:2 benzyl alcohol to benzyl benzoate (BABB) after which they were scanned. OPT scanning was performed using a custom microscope with sample positioning, rotation, and imaging controlled by purpose-built software OPTimum. Fluorophores were excited with an Exfo Xcite 120W Mercury Arc Lamp and images were captured with a Roper Coolsnap HQ2 camera. Semrock filter cubes were used to distinguish emission spectra from flurophores with wavelengths around 488, 568, and 647nm. The images were captured at every 0.9° rotation and averaged twice. The compiled image stack was then reconstructed using nRecon (Skyscan, Kartuizersweg, Kontich, Belgium) and imaged and rendered in Imaris (Bitplane AG, Zurich, Switzerland). Kidneys were imaged and rendered on the same settings. For volume analysis, surfaces were rendered in 0.5μm increments for greater accuracy. For visualisation, surfaces were rendered to 1.5μm. Tip volume calculations are based on average values for >1400 tips/kidney and variation is indicated as the standard error of the mean.

Results

Morphological changes occur within the peripheral cortex during the first six postnatal days

The histology of the peripheral renal cortex was examined using thin sections of mouse kidneys from P0 (birth) to P6 (Figure 1). During the first six postnatal days, profound morphological changes occurred within the most superficial layer of the kidney. To assess the maturity of the superficial cortex, PAS staining was used to highlight both renal tubular basement membranes and the brush border of developing proximal tubules. A region of tissue lacking differentiated proximal tubules, the nephrogenic zone, was present underneath the renal capsule up to P4. During this period, its size remained constant at about 60μm thick (Figure 1a–c). However, by P6 there were differentiated tubules extending right to the edge of the cortex and the nephrogenic zone was no longer visible (Figure 1d). During the first six days, the total cortex thickness increased between P0 to P2 (206 ± 24 vs 264 ± 19 μm) but remained unchanged between P2 to P4 before undergoing another growth from P4 to P6

(271 ± 22 vs 309 ± 25 μm). Analysis of thin cortical sections of plastic embedded kidneys stained with toluidine blue revealed that at P0 and P2 all stages of nephron formation were present in the nephrogenic zone, including cap mesenchyme, pretubular aggregates and early nephrons (renal vesicles, comma-shaped bodies and S-shaped bodies). At P0, the ureteric tips appear to be surrounded by cap mesenchyme (Figure 1e). However by P2, only a thin layer of cells remained between the ureteric tips (UT) and the periphery of the kidney (Figure 1f). This had disappeared by P4 (Figure 1g). By P4, there were very few renal vesicles (RV) detected with most structures representing more mature nephrons. No remaining RVs were detected at P6 (Figure 1g). Unlike earlier timepoints, renal corpuscles (glomeruli) of capillary loop stage nephrons were present in the uppermost layer of the cortex at P4 (Figure 1g) and had differentiated into more mature nephrons at P6, as evidenced by their PAS-stained proximal tubules (Figure 1d). Overall, histological examination suggests cessation of nephrogenesis (defined by evidence for new MET events) occurs between P2 and P4, as previously described (Hartman et al, 2007), together with a novel relationship between the ureteric tips and both the surrounding nephrons and the edge of the kidney, also previously predicted but not demonstrated by previous studies (Hartman et al, 2007).

Loss of cap mesenchymal identity precedes loss of ureteric tip identity during cessation of nephrogenesis

It has previously been proposed that the loss of an ability to form nephrons results from a depletion of the nephron progenitors within the cap mesenchyme rather than the loss of a competent ureteric tip compartment (Hartman et al, 2007). To investigate the changes in identity of these two compartments across the immediate postnatal period, SISH was performed for well characterized markers of CM (*Cited1, Meox2, Crym, Eya1, Six2*) and ureteric epithelium (*Wnt11, Ret, Wnt9b*). *Wnt11* and *Ret* expression was visible from E15.5 to P2, but either only weakly expressed (*Wnt11*) or lost (*Ret*) by P4 (Figure 2). At both E15.5 and P0, *Wnt9b* was expressed along the ureteric epithelium but did not extend to the very tip of the ureteric ampullae (Figure 2). However, *Wnt9b* expression extended more distally into the ureteric tips at P2 to P4. *Wnt9b* was absent from ureteric tip structures at P6 (Supplementary Figure S1). Of particular interest was a change in the morphological relationship between the ureteric tips and RVs at P2 to P4, where two RVs could be seen associated with a single very thinly-shaped ureteric tip (see Figure 2, *Wnt11* at P2). In addition at this time (P2-4), ureteric tips with large open lumens were occasionally observed (see Figure 2, *Meox2* at P2-4). *Wnt11* and *Wnt9b* were also expressed in other renal structures at E15.5 and in the neonatal kidney (Supplementary Figure S1).

In contrast to the loss of UT marker expression between P4-P6, CM markers showed a loss of expression earlier, between P2-P4 (Figure 2). Expression of CM markers suggested both a reduction in area and location of the CM at P2 compared to that seen at E15.5 and P0. Most notably, CM genes were no longer evident in the region peripheral to the UT (ie, between UTs and the edge of the kidney), with the majority of expression seen lateral to the UTs (see Figure 2, *Cited1, Meox2, Crym* at P2). While all cap markers were absent from the kidney at P4-6 (Supplementary Figure S1), the weak expression of some CM genes, including *Eya1* and *Six2*, was seen in early nephron structures from P2 (Figure 2).

The *Six2* gene is strongly associated with the nephron progenitor compartment. Lineage tracing using *Six2* validated the CM as the source of all nephron epithelia with the exception of collecting duct (Kobayashi et al, 2008) and deletion of this gene resulted in premature differentiation of the CM (Self et al, 2006), implicating *Six2* in CM self-renewal. Given the apparent unexpected expression of this gene in early nephrons at P2, we examined this further using immunofluorescence for Six2 protein in conjunction with the basement membrane marker Collagen IV (Figure 3a–d; (Supplementary Figure S2). Whilst the strong gene expression of *Six2* seen in CM at E15.5 and P0 CM (Figure 2) was replicated by expression of the protein (Figure 3a, b), high levels of Six2 protein were present within renal vesicles at P2, as evidenced by the presence of a Collagen IV-positive basement membrane and an internal lumen (Figure 3c). Indeed, Six2 protein was also present at low levels in E15.5 and P0 renal vesicles (Figure 3a, b). By P4, Six2 protein was absent from the kidney (Figure 3d), as was expression of the gene (Figure 2). To examine whether the CM is being replaced by early nephrons at P2, immunofluorescence was performed for the G1/S phase-specific cell cycle marker CyclinD1 (Ccnd1) in conjunction with Collagen IV (Figure 3e–h). We have previously shown differential expression of *Ccnd1* within the distal renal vesicle (Georgas et al, 2009). This same polarized pattern could be seen at P0 and P2 (Figure 3e, g). At P4, *Ccnd1* expression was seen in S-shaped bodies (SSB) and older nephrons. Of particular note, based on the polarized expression of *Ccnd1*, was the observation of “rotated” RVs and S-shaped bodies close to the edge of the kidney from P2 to P4. These structures showed distal-proximal polarity parallel with the surface of the kidney (Figure 3g, h), in contrast to early nephron orientation in the embryonic and P0 kidney (proximal-distal polarity perpendicular to the kidney surface) (Figure 3e, f).

While Six2 has been regarded as critical for CM self renewal, even during development the domain of *Six2* gene expression has been reported to extend beyond that of other CM genes, including *Cited1* and *Meox2* (Mugford et al, 2009). These observations suggest heterogeneity within this compartment potentially representing the presence of CM subpopulations, or a cellular continuum, varying in degree of stemness versus commitment to differentiation (Mugford et al, 2009; Hendry et al, 2011). We show here the clear presence of Six2 protein in early nephrons at P2 (Figure 3) and gene expression analyses of both Six2 and Eya1 also suggest the presence of gene expression in early nephrons (Figure 2). To investigate whether the phenomenon of unexpected CM gene expression in early nephrons similarly subdivided CM markers, collagen IV immunohistochemistry was performed over SISH of either *Meox2* or *Six2* (Supplementary Figure S3). Unlike *Six2*, which was weakly expressed in RV even at P0 and continuing at P2, *Meox2* did not show expression in early nephrons at either timepoint, potentially reflecting its more restricted domain of CM expression during embryonic development. However, the site of *Meox2* expression at P2 was located lateral to the ureteric tips, reflecting the shift in relative location of cap mesenchyme with respect to ureteric epithelium (Supplementary Figure S3). Perdurance of GFP protein after loss of gene expression will occur in GFP reporter mice and can confuse interpretation of biology if the half-life of the GFP extends beyond that of the endogenous protein encoded by the gene it is reporting. Brunskill et al (2011), using Crym-GFP mice, showed GFP fluorescence within the renal vesicles around P2, while our analysis of the expression of this gene suggests a restriction to the CM (Figure 2). However, this may genuinely reflect the

persistence of the Crym protein within the RV. Certainly, the presence of Six2 protein in RV is supported by both SISH and immunofluorescence (Figure 2, Figure 3).

Spatial relationships between forming nephron and ureteric tip change during postnatal nephrogenesis

During embryonic kidney development, nephrons characteristically arise on the underside of the ureteric tip, in close proximity to the ureteric trunk, with one renal vesicle arising for each tip formed. We next examined whether nephrons formed during this postnatal period showed the same molecular patterning as those that develop during embryonic nephrogenesis (Figure 4). This also allowed the examination of the spatial relationship between the final nephrons formed and the ureteric epithelium, and to further investigate the rotated polarity seen in postnatal nephrons at P2 to P4 (Ccnd1 IF, Figure 3). SISH was performed for genes previously described as marking the different domains of the polarizing embryonic renal vesicle (Georgas et al, 2009). Genes included those marking the distal (domain closest to the ureteric tip; *Lhx1*, *Dll1*, *Wnt4*) or proximal renal vesicle (domain furthest from the ureteric tip; *Wt1*, *Tmem100*), as well as non-polarised nephron genes (*Cdh4*, *Sox9*) (Figure 4). All genes examined were expressed in the early nephrons from P0 to P4 and were absent from the nephrogenic zone at P6 (Supplementary Figure S4). By P2, gene expression patterns suggested an altered location of the early nephrons relative to the adjacent ureteric epithelium and a change in orientation with respect to the periphery of the kidney. Of note, *Wnt4* expression was weakly apparent throughout the cap mesenchyme from P2 and strong *Tmem100* expression in cap mesenchyme was seen as early as P0 (Figure 4). This provides evidence that as early as P0 the cap mesenchyme has committed to nephron formation. While most genes maintained the anticipated location of expression, all early nephron genes were detected closer to the surface of the kidney and renal vesicles were seen at the ureteric tip ends (P2, P4), rather than adjacent to the ureteric trunk underneath the ureteric tips (Figure 4). The rotation of the proximal-distal axis of polarity in postnatal RVs is demonstrated by the expression patterns of *Dll1* in renal vesicles at E15.5 and P4 (Figure 5). This rotated axis of polarity in the postnatal kidney was also observed in SSB (Figure 5).

Of the non-polarised nephron genes examined, *Sox9*, was expressed both in the ureteric tip and in early nephrons (RV-SSB) and both this gene and *Cdh4* (nephron-specific) showed an apparent upregulation in their early nephron expression at P4. In the P6 kidney, there appeared to be no remaining early nephron structures present. With the exception of *Tmem100* and *Wnt4*, the early nephron genes examined in this study are known to continue to be expressed in more mature nephrons after S-shaped body stage (Georgas et al, 2009). At P6, the expression of these genes therefore became restricted to either more mature nephron segments (*Wt1* in podocytes, *Dll1* in loop of Henle) or non-nephron tissues (*Wnt4* in collecting ducts and interstitium, *Sox9* in collecting duct) (Supplementary Figure S4).

Three dimensional imaging and modeling of cessation of nephrogenesis reveals changes in the terminal ureteric epithelium and nephron position and number

We have previously defined the relationship of the ureteric tip and the forming nephrons during midgestation using 3D modeling (Georgas et al, 2009). To compare this process with nephrogenesis during the neonatal period, immunofluorescence of serially sectioned P2

kidneys was performed. Serial images collected by fluorescent microscopy were then used to reconstruct a three dimensional model of the terminal nephrons forming around individual branches of the ureteric tree. All structures other than the ureteric epithelium and their associated nephrons were excluded. Renal vesicles (red) were rendered a different color to older nephrons (white) to clearly view the last nephrons being formed (Figure 6). At E15.5, both renal vesicles and more mature nephrons are located underneath the UT and are attached to the tip ends, with only one nephron attached per tip (Georgas et al, 2009). However, modeling at P2 revealed numerous (up to 5) nephrons attached to each tip (Figure 6 and Supplementary Movies 1–3). RVs were seen at the ends of the UTs, rather than underneath them and an altered UT shape was observed, with a dramatic thinning at the UT ends (see Figure 6, yellow arrows in a, e, h, i). The more mature nephrons (SSB-mature stage IV nephrons) that had formed earlier than the RVs at P2, were still seen underneath the UTs. Older nephrons were attached to the ureteric epithelium underneath other younger nephrons attached to the same termini of the ureteric tips (Figure 6h, l). To examine structural changes in the ureteric tip epithelium on a broader scale, optical projection tomography (OPT) was performed on whole P0 and P2 kidneys using immunofluorescence for the ureteric epithelial marker, CalbindinD28K (Figure 7). At P0, clear ampullae were visible at the tips of the ureteric epithelium (Figure 7a, b). However, within 48 hours, most tips had developed an irregular shape and showed numerous indentations, likely representing sites of fusion with adjacent early nephrons (not expressing CalbindinD28K) (Figure 7c, d). This star-shaped pattern also suggests a wave of final ectopic nephron formation events. Volumetric analysis of the rendered tips revealed a 35% reduction in mean tip volume between P0 and P2 (P0 1075±28μm^3, P2 705±17μm^3; $p<0.0005$), indicating that structural changes within the ureteric epithelium accompany this final burst of nephrogenesis. To further investigate the relationship between tips and nephrons at this time, serial thin sections of P2 kidneys were examined (Figure 7 e–g). In agreement with the 3D modeling, multiple nephrons showed patent connections with the same ureteric epithelium (Figure 7 e–g). While the final shape of the ureteric epithelium may be interpreted as ectopic branching, we have shown previously that Calbindin 28KD protein is excluded from the connection point with the ‘invading’ RV (Georgas et al, 2009) and our analysis overall is best interpreted as multiple points of fusion rather than additional branching.

Evidence for gradual depletion of the nephron progenitor population

It is not known what initiates this last wave of nephrogenesis; it may result from an active trigger or reflect a gradual depletion of the nephron progenitor population over time. To investigate this further, immunofluorescence was used to detect Six2, phospho-histone H3 (mitosis-specific cell cycle marker) and CalbindinD28K (ureteric epithelium marker) proteins within the nephrogenic zones of E15.5, P0 and P2 kidneys). Quantitation of $Six2^+$ cells per ureteric tip and percentage of $Six2^+$ cells undergoing mitosis were determined. The average number of $Six2^+$ cells per tip was steady between E15.5 and P0 (E15.5 37.5±1.7, P0 35.8±1.1; ns), but had declined by one third by P2 (P0 35.8±1.1, P2 24.1±0.6; $p<0.0005$). The rate of proliferation within the Six2 compartment significantly dropped between E15.5 and P0 (4.5±0.7 to 2.4±0.3; $p<0.05$). After P0, a non-significant increase in the percentage of $Six2^+$ cells in mitosis was noted (2.4±0.3 to 3.8±0.5; $p>0.05$). However, there was difficulty determining which $Six2^+$ cells represented CM and which had already developed

into early nephrons, as demonstrated in Figure 3. This data is suggestive of a gradual depletion in size and rate of proliferation within the cap mesenchyme.

Discussion and conclusion

In this study, we sought to spatially characterize the last wave of nephrogenesis at high resolution using both gene and protein expression. We present evidence for a burst of nephron formation evident from P2 and almost complete by P4. This agrees with previous studies both suggesting a late wave of nephrogenesis (Hartman et al, 2007; Brunskill et al, 2011). While the ureteric tips no longer maintain normal ureteric tip identity by P4, the loss of cap mesenchyme identity appears to precede this event with evidence for *Wnt4* induction within this compartment by P2. By P6, nephron formation has ceased and all nephrons have fused to, and display lumens contiguous with, the adjacent ureteric epithelium. Notably, the last burst of nephron formation involved novel positioning of early nephrons such that multiple events occur around a single ureteric tip. 3D modeling of the nephrogenic zone confirmed this novel spatial relationship during cessation of nephrogenesis with the final ureteric tips being surrounded by multiple nephrons (up to 5) and displaying an abnormally shaped and often dilated ampulla. This suggests a synchronized wave of fusion with each of the forming nephrons. These findings are summarized in Figure 9.

The novel spatial relationships observed across cessation of nephrogenesis represent a dramatic alteration in the spatial and molecular context of the nephrogenic niche. Such a change has been implied from previous studies (Hartman et al, 2007) but here we provide clear modeling of this process. While such a spatial relationship is not observed during normal embryonic nephrogenesis in the mouse, it appears reminiscent of that seen in the presence of Sox8/Sox9 mutations where nephrogenesis ceases prior to birth (Reginensi et al, 2011). We have previously proposed that the CM population, rather than representing a homogenous region with clear borders between itself and the forming nephron compartment, can be viewed as a continuum (Hendry et al, 2011). Indeed the population has been shown to display a heterogeneous gene expression (Mugford et al, 2009). The unexpected expression of *Wnt4*, a gene required for MET, and *Tmem100*, a distal RV marker, within the cap mesenchyme, coupled with the unexpected location of cap mesenchyme genes such as *Six2* and *Eya1* in early nephrons is most easily explained as an accelerated induction of differentiation throughout the cap mesenchyme from P0. This may result from changes in spatial relationships between components of the nephrogenic niche that would undoubtedly alter growth factor gradients within that niche, potentially resulting in a contraction of this CM continuum. The observation of high levels of Six2 protein (although only low *Six2* gene expression) within neonatal renal vesicles does suggest that Six2 alone is not sufficient to maintain self renewal. This was also observed by Brunskill et al (2011), although this is in contrast to what has previously been proposed (Self et al, 2006). Wnt9b is known to be critical in the induction of nephron formation (Carroll et al, 2005), although it has been recently shown to also regulate cap mesenchymal self renewal with the balance of these activities dependent upon the context of the receiving cell population (Karner et al, 2010). *Wnt9b* expression appears to extend closer to the ends of the ureteric tips during the first 4 postnatal days. Alterations in the local concentration of this ligand alone may be sufficient to induce a shift between support of CM self renewal and induction of pretubular aggregates.

Certainly an upregulation of *Wnt4* within cap mesenchyme may result from such alterations to *Wnt9b* expression. However our data do not support Six2 as being the key contextual cap mesenchymal protein determining the Wnt9b response.

The mechanism initiating cessation of nephrogenesis is not known, however a number of possible explanations have been proposed (Brunskill et al, 2011; Hendry et al, 2011). The first evokes an active differentiation trigger at/near birth. Based on changes in the expression of glycolytic genes between P0 and P2, Brunskill et al 2011 proposed that an increase in oxygen tension at birth may represent a possible active trigger for cessation of nephrogenesis. However, an alternative would be the gradual exhaustion of the nephron progenitor population over time, potentially due to changes in spatial relationships between different cell-types within the nephrogenic niche, such that ultimately self-renewal of the nephron progenitors ceases to occur (Brunskill et al, 2011; Hendry et al, 2011). Our analyses suggest that the CM population is declining in size through development (Figure 8). This supports this latter model in which there is gradual change in this spatial arrangement occurring throughout development. This may culminate in exhaustion of the cap mesenchyme potentially without a single triggering event. Of note, the pattern of Crym GFP present within the nephrogenic zone at P3 presented in Brunskill et al (2011) is most closely aligned to the morphology and pattern of Six2 protein present in the nephrogenic zone at P2 in our study. This discrepancy in timing between these studies is likely to stem from the fact that mothers were allowed to birth naturally in this study whereas Brunskill et al (2011) performed C-section at E18.5, a gestational age 12–36 hours earlier than in our study. The fact that this resulted in an offset in the timing of cessation would also argue against a parturition-based active trigger as such a trigger would override gestational age.

The relevance of these studies to cessation of nephrogenesis in human kidney development is not clear. The literature tends to refer to Hinchcliffe et al (1991) to conclude that nephron endowment in the human ceases around 36 weeks of gestation. There is a plateauing of nephron number at this time based upon Cavlieri quantitation. If this is the case, a parturition-based active trigger would not be applicable to humans. However, other studies report continued nephrogenesis up to and even beyond birth in humans (Faa et al, 2010;Gruenwald 1940), making a common parturition-based trigger feasible for both humans and mice. Alternatively, both may be explained via a gradual decline in CM size resulting in a failure to continue to support self renewal. Clarification of mechanism in both organisms will be critical not only to understand the basis of the wide variation in nephron number seen between individuals, but also to potentially intervene to alter this process under conditions of severe intrauterine growth retardation and prematurity.

Supplementary Material

Refer to Web version on PubMed Central for supplementary material.

Acknowledgements

This work was funded by the NIDDK, National Institute of Health, USA (DK070136). We acknowledge Drs. Ian Smyth, Kieren Short, Nick Hamilton and James Springfield for technical assistance and advice in establishing OPT

and applying Imaris. ML is a Principal Research Fellow of the National Health and Medical Research Council of Australia.

References

Boyle S, Misfeldt A, Chandler KJ, Deal KK, Southard-Smith EM, Mortlock DP, Baldwin HS, de Caestecker M. Fate mapping using Cited1-CreERT2 mice demonstrates that the cap mesenchyme contains self-renewing progenitor cells and gives rise exclusively to nephronic epithelia. Dev Biol. 2008; 313(1):234–245. [PubMed: 18061157]

Brenner BM, Anderson S. The interrelationships among filtration surface area, blood pressure, and chronic renal disease. J Cardiovasc Pharmacol. 1992; 6(19 Suppl):S1–7.

Brunskill EW, Lai HL, Jamison DC, Potter SS, Patterson LT. Microarrays and RNA-Seq identify molecular mechanisms driving the end of nephron production. BMC Developmental Biology. 2011; 11:15. [PubMed: 21396121]

Burn SF, Webb A, Berry RL, Davies JA, Ferrer-Vaquer A, Hadjantonakis AK, Hastie ND, Hohenstein P. Calcium/NFAT signalling promotes early nephrogenesis. Dev Biol. 2011; 352(2):288–98. [PubMed: 21295565]

Carroll TJ, Park JS, Hayashi S, Majumdar A, McMahon AP. Wnt9b plays a central role in the regulation of mesenchymal to epithelial transitions underlying organogenesis of the mammalian urogenital system. Dev Cell. 2005; 9:283–292. [PubMed: 16054034]

Costantini F, Kopan R. Patterning a complex organ: branching morphogenesis and nephron segmentation in kidney development. Dev Cell. 2010; 18(5):698–712. [PubMed: 20493806]

Faa G, Gerosa C, Fanni D, Nemolato S, Locci A, Cabras T, Martinelli V, Puddu M, Zaffanello M, Monga G, Fanos V. Marked interindividual variability in renal maturation of preterm infants: lessons from autopsy. J. Maternal-Fetal and Neonatal Med. 2010; 23(S3):129–133.

Georgas KM, Rumballe BA, Valerius MT, Chiu HS, Thiagarajan RD, Lesieur E, Aronow BJ, Brunskill EW, Combes AN, Tang D, Taylor D, Grimmond SM, Potter SS, McMahon AP, Little MH. Analysis of early nephron patterning reveals a role for distal RV proliferation in fusion to the ureteric tip via a cap mesenchyme-derived connecting segment. Dev Biol. 2009; 332(2):273–286. [PubMed: 19501082]

Grieshammer U, Cebrian C, Ilagan R, Meyers E, Herzlinger D, Martin GR. FGF8 is required for cell survival at distinct stages of nephrogenesis and for regulation of gene expression in nascent nephrons. Development. 2005; 132(17):3847–3857. [PubMed: 16049112]

Gruenwald P, Popper H. The histogenesis and physiology of the renal glomerulus in early postnatal life. J Urol. 1940; 43:452–466.

Hartman HA, Lai HL, Patterson LT. Cessation of renal morphogenesis in mice. Dev Biol. 2007; 310:379–387. [PubMed: 17826763]

Hendry C, Rumballe BA, Moritz K, Little MH. Defining and redefining the nephron progenitor population. Pediatric Nephrology. 2011 (EPub ahead of print).

Hinchliffe SA, Sargent PH, Howard CV, Chan YF, van Velzen D. Human intrauterine renal growth expressed in absolute number of glomeruli assessed by the disector method and Cavalieri principle. Lab Invest. 1991 Jun; 64(6):777–84. [PubMed: 2046329]

Hughson M, Farris AB 3rd, Douglas-Denton R, Hoy WE, Bertram JF. Glomerular number and size in autopsy kidneys: the relationship to birth weight. Kidney Int. 2003; 63:2113–2122. [PubMed: 12753298]

Kobayashi A, Valerius MT, Mugford JW, Carroll TJ, Self M, Oliver G, McMahon AP. Six2 defines and regulates a multipotent self-renewing nephron progenitor population throughout mammalian kidney development. Cell Stem Cell. 2008; 3(2):169–181. [PubMed: 18682239]

Kopan R, Cheng H-T, Surendran K. Molecular insights into segmentation along the proximal-distal axis of the nephron. J. Amer. Soc. Nephrol. 2007; 18:2014–2020. [PubMed: 17568016]

Luyckx VA, Brenner BM. The clinical importance of nephron mass. J Am Soc Nephrol. 2010; 21(6): 898–910. [PubMed: 20150537]

McMahon AP, Aronow BJ, Davidson DR, Davies JA, Gaido KW, Grimmond S, Lessard JL, Little MH, Potter SS, Wilder EL, Zhang P, GUDMAP project. GUDMAP: the genitourinary developmental molecular anatomy project. J Am Soc Nephrol. 2008; 19(4):667–71. [PubMed: 18287559]

Merlet-Benichou C, Gilbert T, Vilar J, Moreau E, Freund N, Lelievre-Pegorier M. Nephron number : variability is the rule. Causes and consequences. Lab Invest. 1999; 79:515–527. [PubMed: 10334563]

Mugford JW, Yu J, Kobayashi A, McMahon AP. High-resolution gene expression analysis of the developing mouse kidney defines novel cellular compartments within the nephron progenitor population. Dev Biol. 2009; 333(2):312–323. [PubMed: 19591821]

Park JS, Valerius MT, McMahon AP. Wnt/beta-catenin signaling regulates nephron induction during mouse kidney development. Development. 2007; 134(13):2533–9. [PubMed: 17537789]

Perantoni AO, Timofeeva O, Naillat F, Richman C, Pajni-Underwood S, Wilson C, Vainio S, Dove LF, Lewandoski M. Inactivation of FGF8 in early mesoderm reveals an essential role in kidney development. Development. 2005; 132(17):3859–3871. [PubMed: 16049111]

Reginensi A, Clarkson M, Neirijnck Y, Lu B, Ohyama T, Groves AK, Sock E, Wegner M, Costantini F, Chaboissier MC, Schedl A. SOX9 controls epithelial branching by activating RET effector genes during kidney development. Hum Mol Genet. 2011; 20(6):1143–53. [PubMed: 21212101]

Self M, Lagutin OV, Bowling B, Hendrix J, Cai Y, Dressler GR, Oliver G. Six2 is required for suppression of nephrogenesis and progenitor renewal in the developing kidney. EMBO J. 2006; 25(21):5214–5228. [PubMed: 17036046]

Stark K, Vainio S, Vassileva G, McMahon AP. Epithelial transformation of metanephric mesenchyme in the developing kidney regulated by Wnt-4. Nature. 1994; 372(6507):679–83. [PubMed: 7990960]

Tanigawa S, Wang H, Yang Y, Sharma N, Tarasova N, Ajima R, Yamaguchi TP, Rodriguez LG, Perantoni AO. Wnt4 induces nephronic tubules in metanephric mesenchyme by a non-canonical mechanism. Dev Biol. 2011; 352(1):58–69. [PubMed: 21256838]

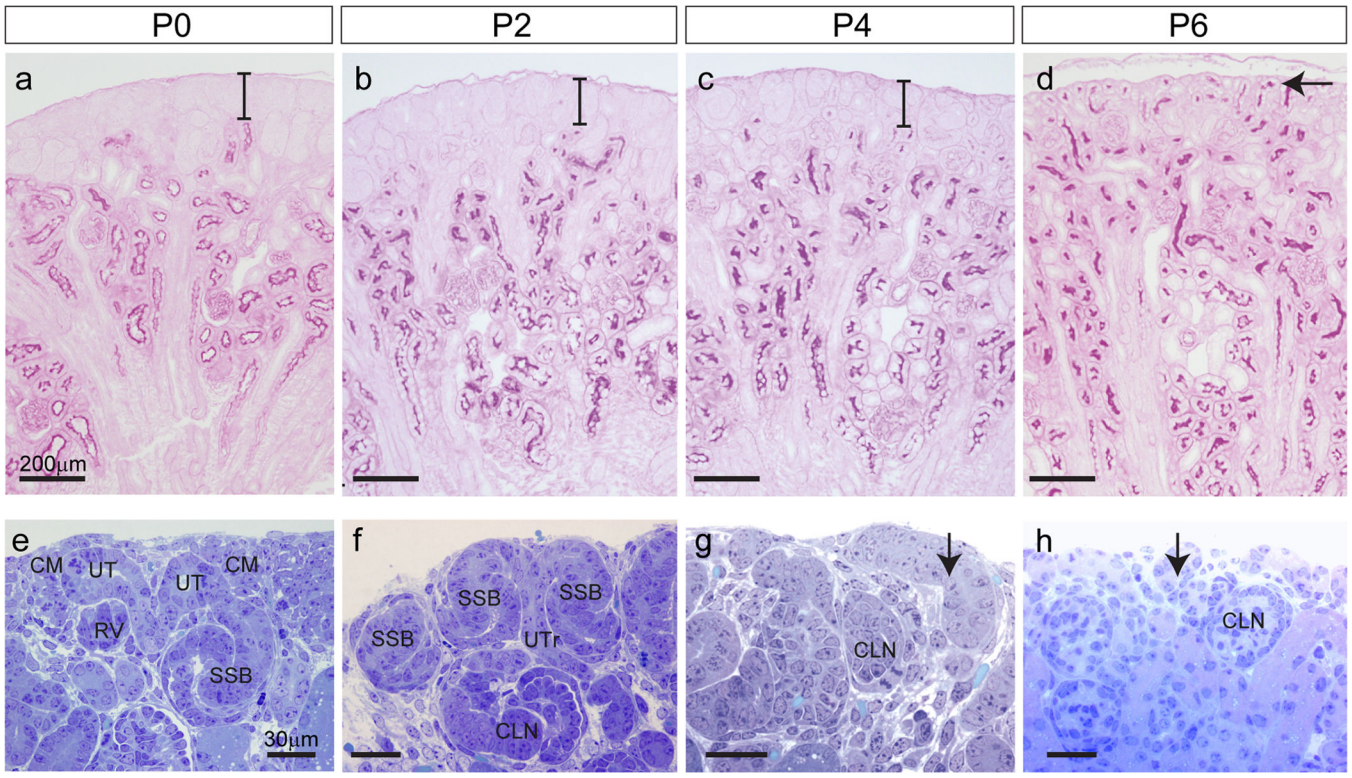

Figure 1. Histology of the peripheral cortex during the first six postnatal days

(a–d) Thin sections stained with PAS (Periodic Acid Schiff's) for glycogen carbohydrates in basement membrane and renal proximal tubule brush border (magenta) from P0-6. The nephrogenic zone, not stained by PAS, is seen at the periphery of the kidney from P0-P2 and remains relatively constant in width during this time (bars in a–c). By P6, PAS stained tubules are seen at the kidney surface as the nephrogenic zone is replaced with the tubules of more mature nephrons (arrow in d). Scale bar in (a) = 100μm. (e–h) Thin sections stained with toluidine blue. At P0, cap mesenchyme (CM) is seen surrounding the ureteric tips (UT) and each UT is attached to a single nephron (e). At P2, early nephrons (RV-SSB) are seen close to the surface of the kidney. A single UT may be attached to more than one nephron (f). At P4 and P6 more mature nephron tubules are seen at the kidney edge (arrows in g–h). Scale bars = 200μm (a–d) and 30 μm (e–h). CM, cap mesenchyme; UT, ureteric tip; RV, renal vesicle; SSB, S-shaped body; UTr, ureteric trunk; CLN, capillary loop nephron.

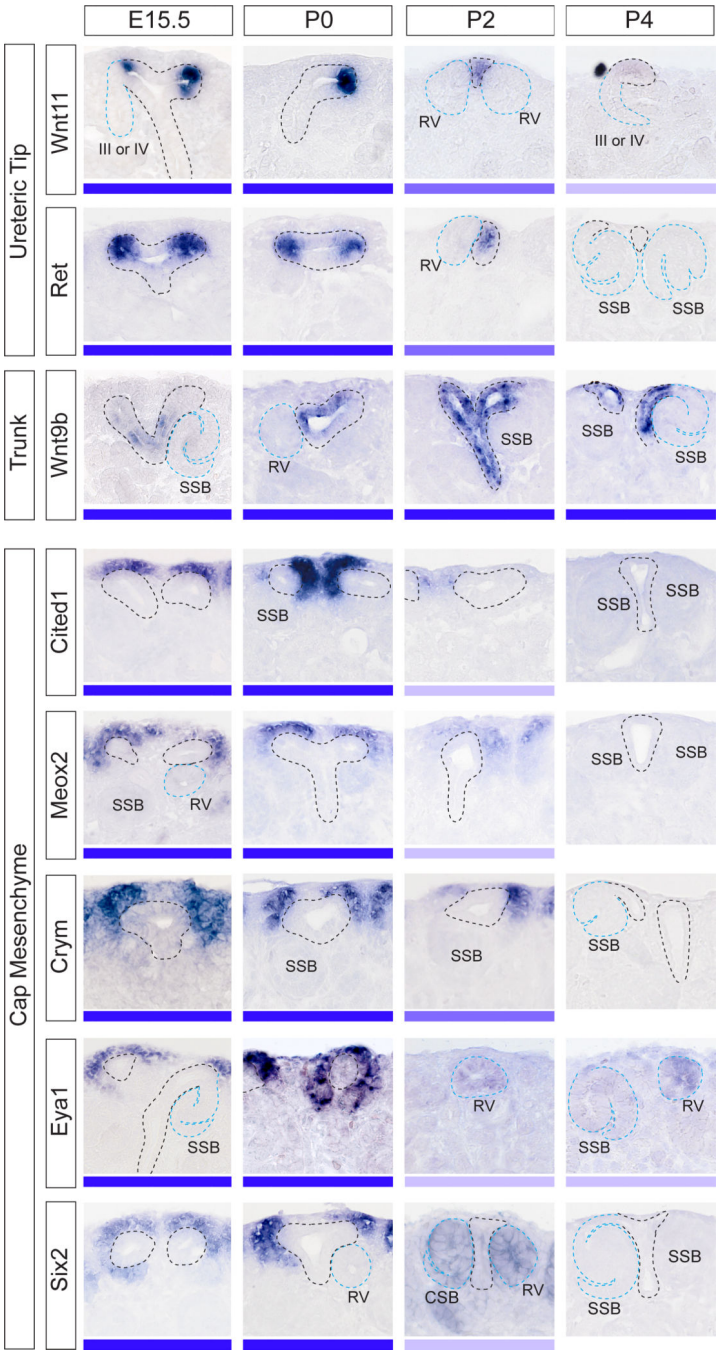

Figure 2. Gene expression implies exhaustion of nephron progenitors precedes loss of ureteric tip identity

Gene expression profiling of ureteric epithelium markers of tip (*Wn11, Ret*) and trunk (*Wnt9b*) and cap mesenchyme markers (*Cited1, Meox2, Crym, Eya1, Six2*) using SISH at E15.5, P0-4. Although Wnt9b is a marker of ureteric trunk, it was detected in the ureteric tip at P2-4. High magnification images of the nephrogenic zone are shown with ureteric tree outlined in black and nephrons outlined in blue. The expression strength (strong-weak) of each gene is represented as a blue bar underneath each image. The expression of ureteric markers in the tip was detectable until P4, whereas CM markers were detectable in the cap

until P2. *Eya1* and *Six2* were present in nephron structures from P2-P4. RV, renal vesicle; SSB, S-shaped body; CLN, capillary loop nephron (Stage III nephron). Additional low magnification images of the entire kidney (E15.5, P0-6) are available in Supplementary Figure S1.

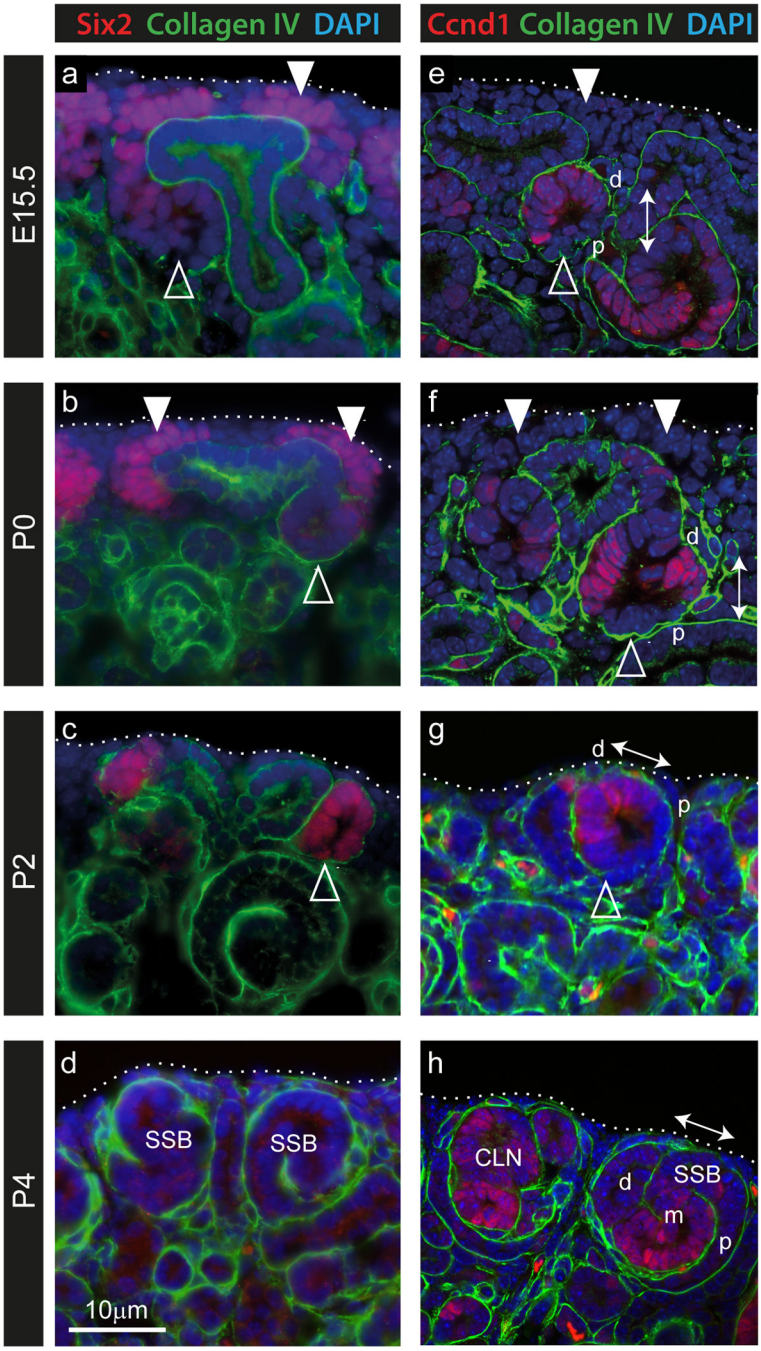

Figure 3. Presence of Six2 and Cyclin D1 proteins within renal vesicles during cessation of nephrogenesis

Immunofluorescence of embryonic and postnatal kidney sections using anti-Six2 (red, ad), anti-Cyclin D1 (Ccnd1; red, e–h) and anti-Collagen IV (green, a–h) antibodies to mark cap mesenchyme, proliferating cells in G1/S phase and basement membrane respectively. At E15.5 and P0, the cap mesenchyme (marked by white arrowheads) could be identified by strong Six2 expression (a, b). As the cap is lost (at P2), Six2 is strongly expressed in early nephrons (marked by open arrowheads) at the ends of the ureteric tips (c). However prior to this stage, weak Six2 expression was also seen in renal vesicles and pretubular aggregates

underneath the tips at E15.5 and P0 (a–c). Ccnd1 displayed polarized expression in the distal renal vesicle in the embryonic kidney (open arrowhead in e), as shown previously (Georgas et al, 2009), which was maintained in distal RVs at P0 to P2 (open arrowheads in eg). In the embryonic and P0 kidney the proximal-distal polarity of early nephrons could be seen perpendicular to the kidney surface (arrow in e–f), however at P2 and P4, these nephrons (RV-SSB) appeared ‘rotated’ as their distal-proximal polarity could be seen parallel to the surface of the kidney (arrows in g–h). The edge of the kidney is outlined. SSB, S-shaped body; CLN, capillary loop nephron; d, distal; m, medial; p, proximal. Low magnification images are available in Supplementary Figure S2.

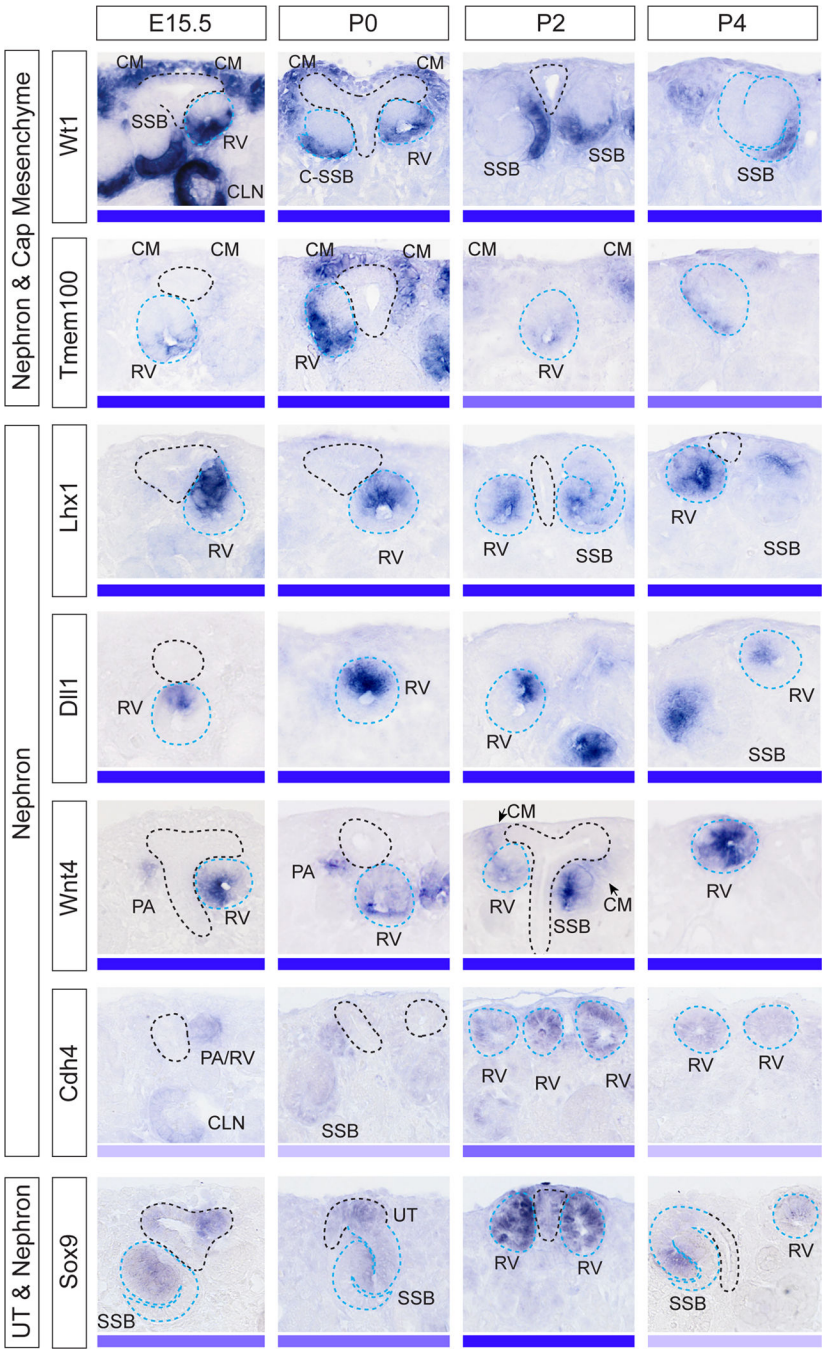

Figure 4. Gene expression of early nephron markers reveal changes in the spatial relationships between the forming nephrons, ureteric tip and kidney periphery during postnatal nephrogenesis

Gene expression profiling of nephron markers using SISH at E15.5, P0-4. Genes included proximal nephron markers (*Wt1, Tmem100*) also present in the cap mesenchyme. Nephron markers included genes marking the distal renal vesicle (*Lhx1, Dll1*) and genes present in both sides of the renal vesicle (*Wnt4, Cdh4*). *Sox9* was present in nephrons as well as in the ureteric tree. High magnification images of the nephrogenic zone are shown with ureteric tree outlined in black and nephrons outlined in blue. The expression strength (strong-weak)

of each gene in early nephrons is represented as a blue bar. The profiling shows that expression of nephron markers was detectable until P4. *Tmem100* weakly expressed in the cap mesenchyme at E15.5 appeared to be upregulated in the cap postnatally, most notable at P0. *Wnt4*, present in nephrons as early as pretubular aggregate stage, appeared to be present in the cap mesenchyme at P2 (arrows), although this mesenchymal expression may be early pretubular aggregates surrounding the P2 ureteric tips. PA, pretubular aggregate; RV, renal vesicle; SSB, S-shaped body; III or IV, stage III or IV nephron epithelia. Additional low magnification images of the entire kidney (E15.5, P0-6) are shown in Supplementary Figure S4.

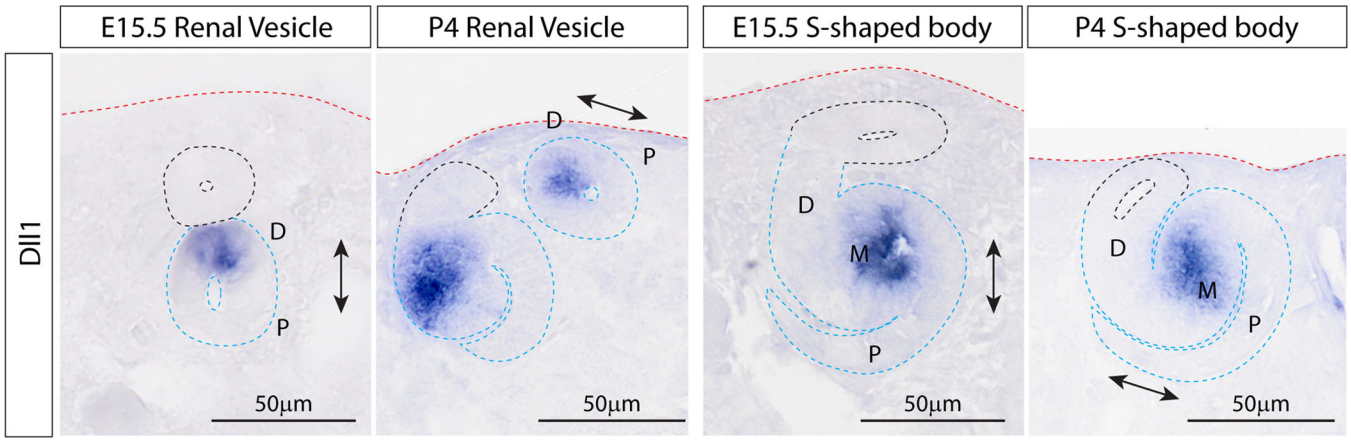

Figure 5. Maintained nephron patterning but altered orientation during cessation of nephrogenesis

Section *in situ* hybridization for *Dll1* in early nephrons shows that polarity in renal vesicles (RV) with respect to the position of the ureteric tip, first demonstrated at E15.5 (Georgas et al, 2009), is maintained by RVs that develop postnatally. However, because the RVs develop in a different location with respect to the ureteric tip (at the tip ends) at P4, rather than underneath the ureteric tips (E15.5), the proximal-distal axis of polarity (arrows) in RVs is rotated in the P4 kidney. This is demonstrated by the expression patterns of *Dll1* (distal RV) in renal vesicles at E15.5 and P4. This rotated axis of polarity in the P4 kidney is also seen in S-shaped bodies, where *Dll1* expression is restricted to a small region within the medial SSB. Ureteric tips (black), nephrons (blue) and the outer edge of the kidney (red) are outlined. Loss of the cap mesenchyme together with the rotated location of the nephrons places them closer to the edge of the kidney at P4. D, distal; P, proximal; M, medial.

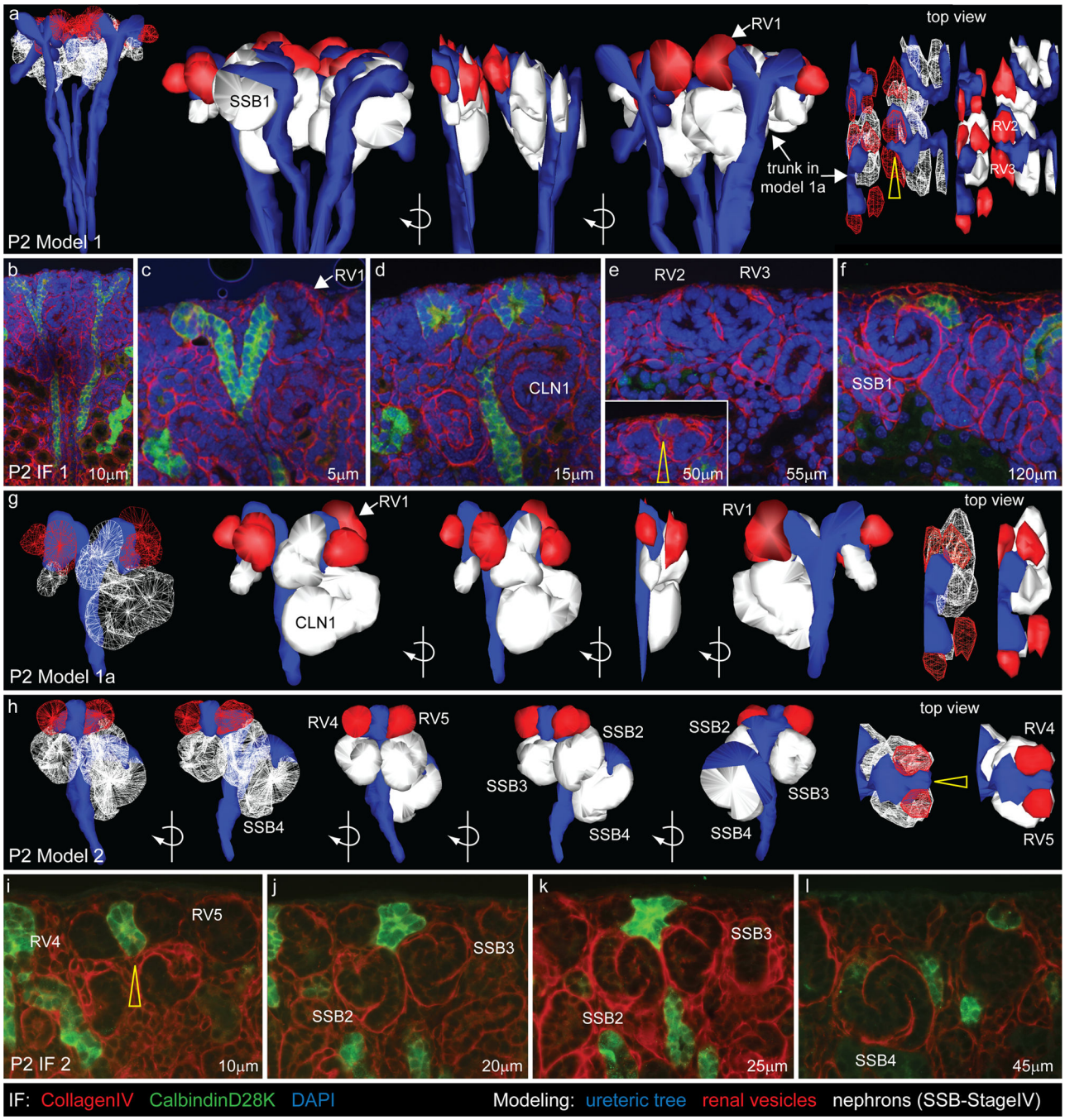

Figure 6. 3D modeling of the nephrogenic zone in the immediate postnatal period

Immunofluorescent labeling of serially sectioned P2 kidneys using antibodies to Collagen IV (basement membrane, red) and CalbindinD28K (ureteric tree, green) was used to model in 3D the spatial relationships between the ureteric tree and nephrons. 3D models (a, g, h) are shown above representative sections (b–f, i–l) and ureteric tree (blue), renal vesicles (red) and older nephron structures (white) have been modeled. Individual nephrons are numbered. Two regions of P2 nephrogenic zone are shown. In model 1 (a) 4 terminal ureteric tree branches and their associated nephrons were modeled. Model 1a (g) is a subset

of Model 1 showing a single ureteric tree terminal branch, one tip is associated with 3 nephrons, the other tip with 4. In model 2 (h), a single terminal branch is shown, with 5 nephrons attached (2 RVs, 3 SSBs). One of these nephrons (SSB4) is attached to the ureteric epithelium below the other nephrons which are attached to the terminal of the ureteric tip (h, l). Altered UT morphology is seen as a thinning at the UT ends (see yellow arrows in top view of models (a, h) and IF (e, i) images). RV, renal vesicle; SSB, S-shaped body; CLN, capillary loop nephron. Movies of the 3D models are available as Supplementary Movie files; Movie 1 (model 1), Movie 2 (model 1a), Movie 3 (model 2).

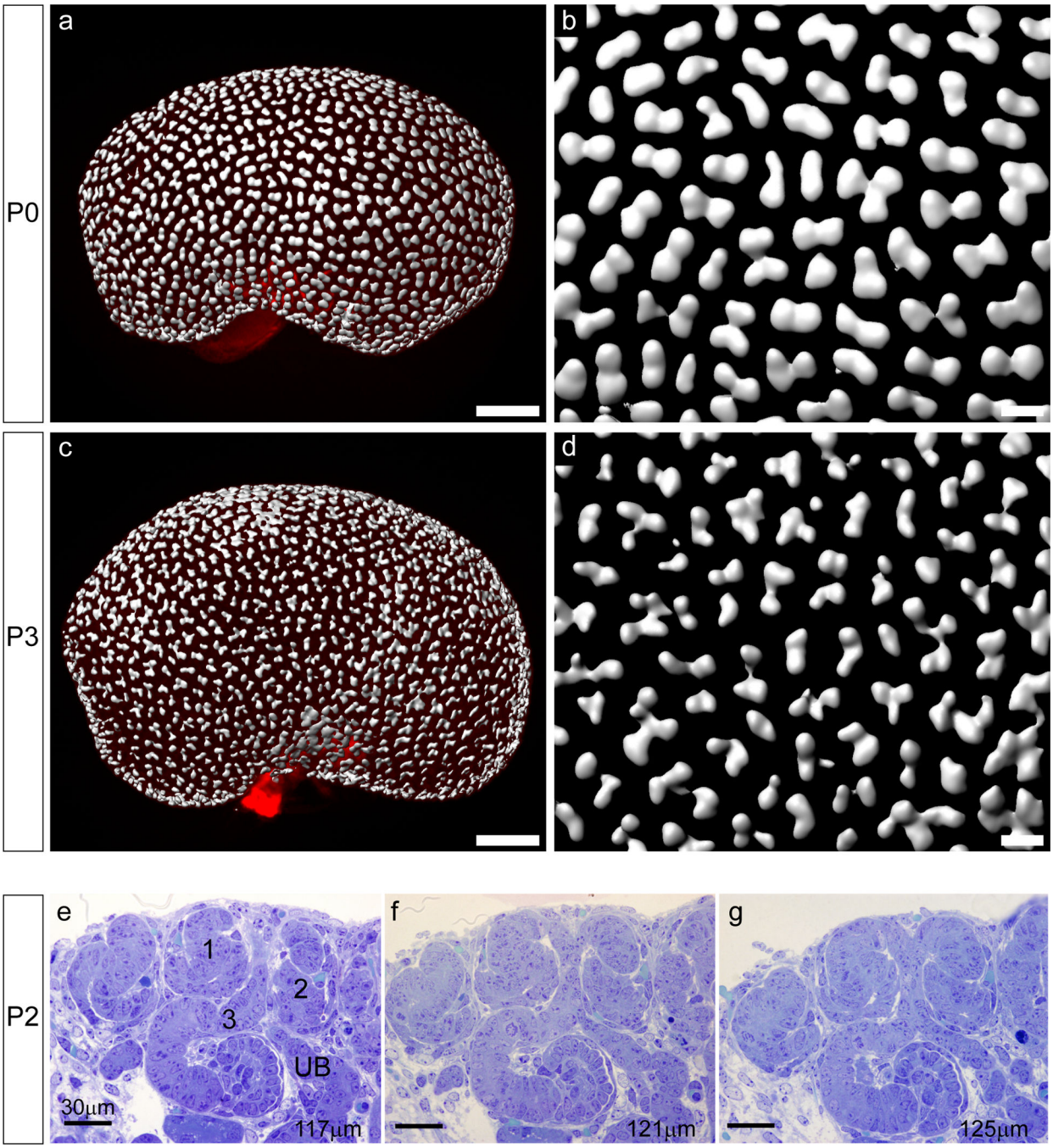

Figure 7. Changes to postnatal ureteric tip morphology as multiple nephrons attach to each tip

(a–d) OPT of P0 and P2 ureteric epithelium performed on kidneys immunofluorescently-labeled with anti-CalbindinD28K antibody. Scale bars a & c = 20 μm; b & d = 100μm. (e–g) Serial thin (4μm) sections of an area of P2 nephrogenic zone stained with toluidine blue. The series shown here demonstrates 3 nephrons (labeled 1–3) attached to the same terminal branch of the ureteric tree (UB), including two S-shaped bodies (1, 2) located at the surface of the kidney and attached to the terminal of the ureteric tip, and a nephron at the capillary

loop stage (3) located underneath nephrons 1 and 2 and attached to the ureteric epithelium below the tip terminal. Scale bar = 30μm.

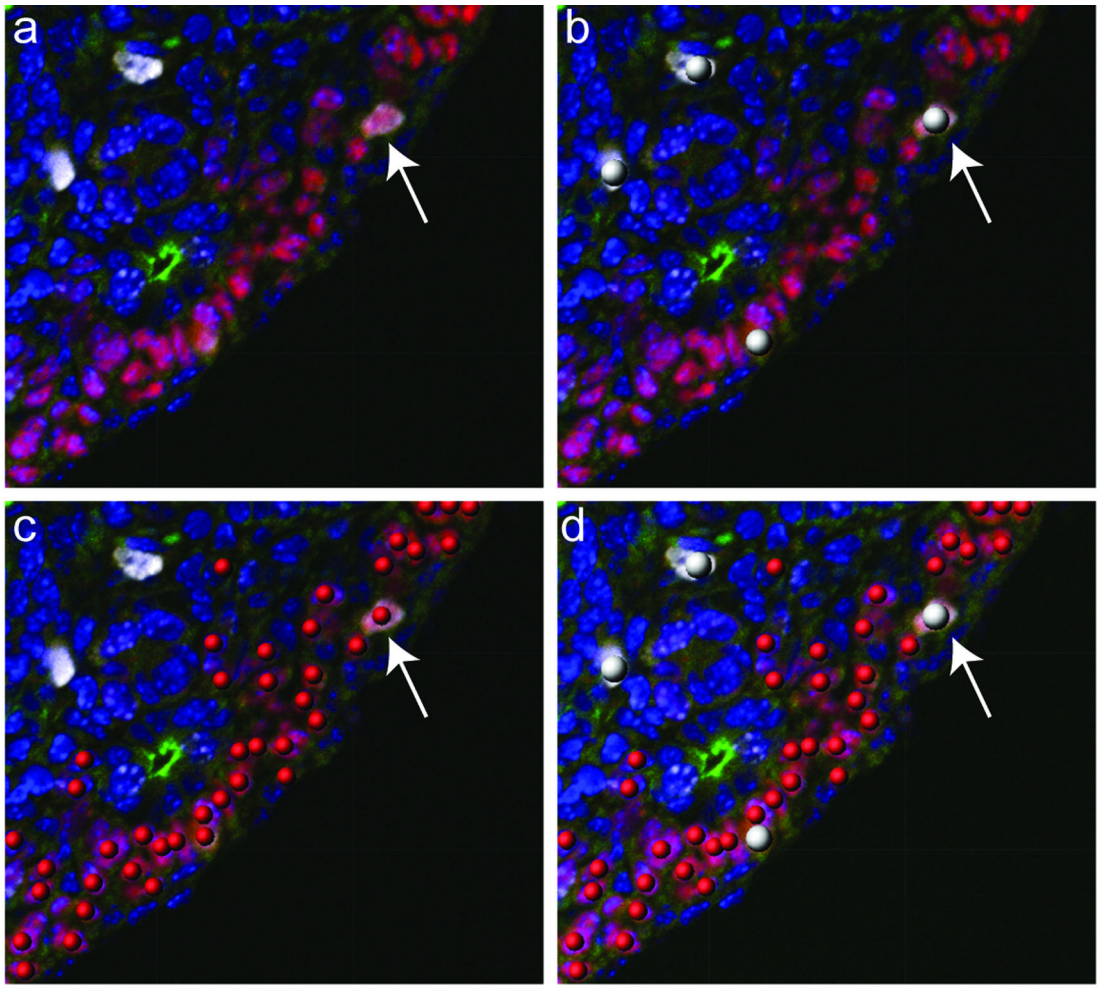

e

Stage	# sections (n)	Total Six2+ cells	%Six2+ cells in mitosis	+/- SEM	Six2+ cells per tip	+/- SEM
E15.5	16	3576	4.5	0.7	37.5	1.7
P0	14	2016	2.4	0.3	35.8	1.1
P2	26	2412	3.8	0.5	24.1	0.6

Figure 8. Quantitative temporal analysis of cellular proliferation in the cap mesenchyme

(a–d) Co-immunofluorescence for Six2 (red, CM), CalbindinD28K (green, UB), pHH3 (white, mitosing cells) and DAPI (blue, nuclei) of kidney sections (a) utilized for spot detection of pHH3+ (b), Six2+ (c) and pHH3+/Six2+ cells (d) performed using spot counting algorithms in BitPlane Imaris. (e) Quantitation of CM/tip and percentage of CM cells undergoing mitosis from E15.5 to P2.

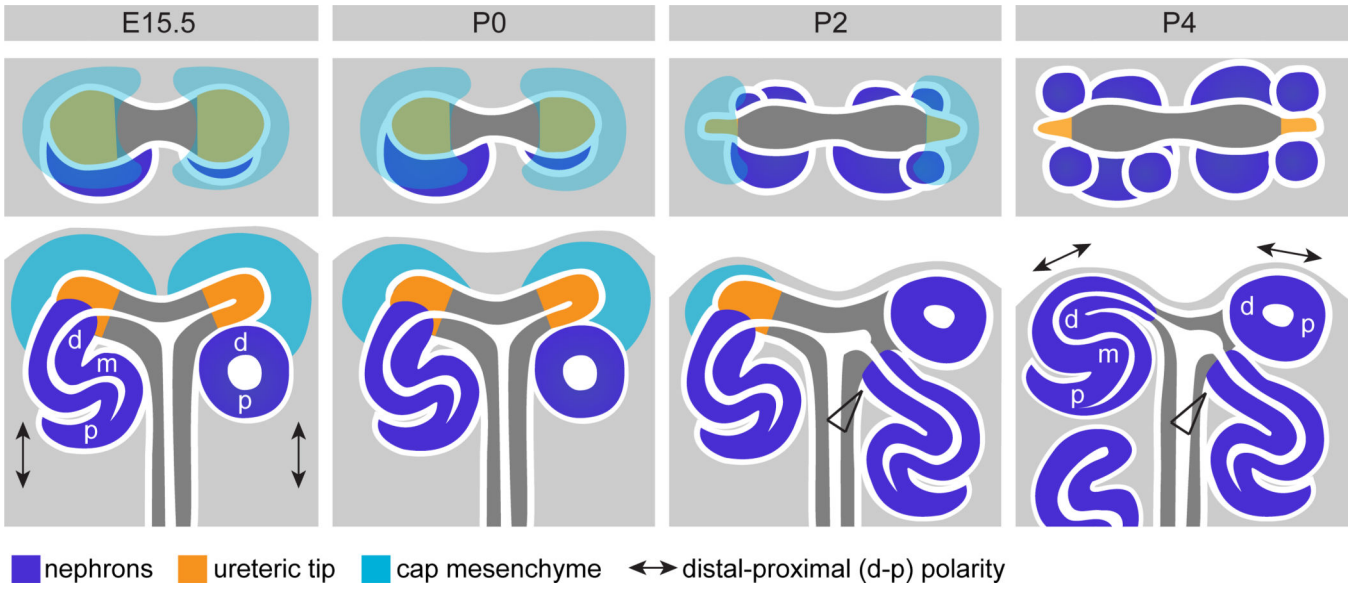

Figure 9. Summary of spatial and molecular changes across the cessation of nephrogenesis

This schematic illustrates the location and spatial arrangement of the cap mesenchyme (green), ureteric tip (orange) and nephron (blue) compartments within the nephrogenic zone at E15.5 and P0-4. A top view and side view are shown for each age. At E15.5, cap mesenchyme is present surrounding each ureteric tip. As nephrogenesis ceases the cap mesenchyme is lost (absent at P4), at which time nephron and tree epithelia are located very close to the edge of the kidney. The molecular identity of the ureteric tip is maintained (yellow) after markers of the cap mesenchyme are lost. Molecular polarity in the early nephron occurs with respect to the position of the adjacent ureteric tip. At E15.5, distal-proximal nephron polarity in the kidney is indicated (arrows) and occurs in this orientation as nephrons develop in a specific location, underneath the ureteric tips (in the 'armpit' of the terminal branches of the ureteric tree). As the cap is lost, new nephrons are formed at the sides of the tip ends and nephron polarity is rotated in the kidney (arrows in P4) as the position of the new nephrons changes. At E15.5, each tip induces the formation of one nephron, postnatally as the cap differentiates into nephrons, multiple nephrons are seen attached to a single tip and at P2, up to 5 nephrons are seen associated with each tip (see top view P4). From P2-4, older nephrons can be seen attached to the ureteric epithelium below younger nephrons attached to the tip ends (arrowheads in P2-4).